Evaluation of abradable seal coating mechanical properties

Xiao Ma, Allan Matthews

Evaluation of abradable seal coating mechanical properties

Xiao Ma, Allan Matthews

Department of Engineering Materials, University of Sheffield, Sheffield S1 3JD, UK

Three proprietary plasma-sprayed coatings, based on Ni–graphite, Al–Si–graphite and Al–Si–polyester, were chosen for evaluation by the use of a (low speed) scratch tester, as a means of assessing the per-formance of abradable coatings. The scratch test behaviour was also correlated with the mechanical properties of the coatings (elastic modulus, microhardness and ultimate tensile strength). The results obtained were compared with those from industrial trials, to ascertain if the scratch test could be used as a relatively cheap and effective alternative to expensive engine trials. We have shown that the Pro-gressive Abradability Hardness, abbreviated below as PAH, can be utilised as a measure of abradability in the scratch test, and can be related to the mechanical properties, in a manner consistent with engine test-bed findings. We have also found that the abradability and the PAH can change with scratch length due, we believe, to coating compression and densification ahead of the slider. In this work, the PAH has been related to coating hardness, ultimate tensile strength and elastic modulus.

Keywords: Abradable seal coatings, Scratch testing, Progressive Abradability, Hardness Abradability

1. Introduction

Turbo-engine efficiency is governed by the maximum pressure and the operating temperature [1]. Particularly in the last two decades the turbomachinery industry has been making every effort to optimise these two crucial factors, for example by enhancing the operating temperature using temperature-tolerant superalloys and thermal barrier coating systems, and incorporating appropriate aerodynamic features. A primary design requirement is to minimise the clearance between the rotating blades and the casing, so that the air can be transferred to the compressor as efficiently as possible to provide thrust and reduce fuel consumption [2]. Abradable seal coatings have achieved great success on this regard and are now been used extensively in both aero-engines and land-based turbo generators [3].

Abradable seal coatings have been engineered to minimise the clearance between blade-tips and casing to enhance gas-turbine performances [1,2]. During operation, gas-turbine blades rotate at a very high speed (typically 3000–10,000 rpm or higher for aero-engines) and may therefore rub the casing due to either thermal expansion, misalignment or rotation-induced strains [2,4]. Abradable seal coatings are applied in between the blade-tips and the casing to prevent such catastrophic contact while maintaining minimum clearance between them. An earlier paper was written by the authors [4] that mainly focused on an investigation of using scratch testing to determine abradability. It will be referred to as "the investigation paper" in the rest of this paper.

In order to achieve the required performance, the optimal microstructure developed typically consists of a metal matrix supplying desirable erosion and oxidation resistance and a solid lubricant phase such as graphite to provide abradability [5,6]. While abradable seal coating materials are usually evaluated using high speed rubbing rigs by replicating the aerodynamics and contact environments inside gas-turbine engines [7] or other forms of alternative laboratory high speed tests [8–12], this paper introduces investigation of several abradable materials using laboratory facilities, including the method of scratch testing to determine their abradability. The Progressive Abradability Hardness (PAH) has been proposed as a measure of abradability and shown to be well-related to other mechanical properties. In the investigation paper [4] this concept was introduced, and the present paper provides more information on the work, and associated modelling.

2. Experimental details and theories

Elastic modulus, microhardness and ultimate tensile strength were measured for the abradable seal coatings. The detailed specimen shapes and dimensions are listed in Table 1.

2.1. Elastic modulus evaluation

An elastic modulus evaluation was performed using a cantilever beam bending test configuration, shown in Fig. 1. The experimental

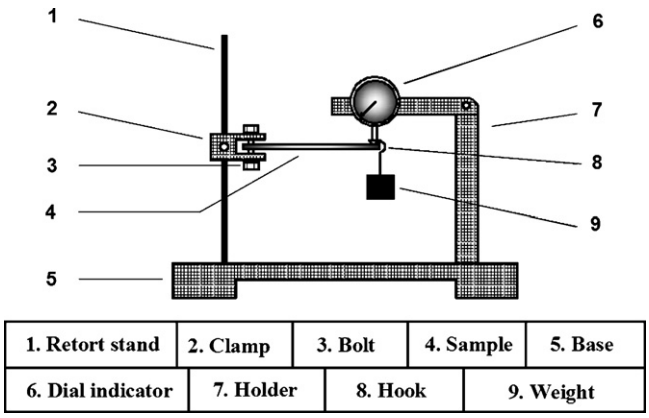

Fig. 1. The cantilever beam bending arrangement used for elastic modulus determination.

setup and derivation of the elastic modulus of coatings have been detailed in the investigation paper [4].

2.2. Microhardness evaluation and finite element simulation

The theories surrounding hardness testing are well known [13,14]; however the plastic deformation which takes place under and around an indenter can be complex and can adversely affect the final hardness value if, for example, the plastic deformation volume incorporates the substrate [15–18]. In film hardness testing, a theoretical treatment aiming at eliminating substrate influence is a necessity. In order to calculate the plastic deformation volume, a rule of thumb [15] and an experimentally validated expression found by Lawn et al. [19] were compared. The rule of thumb states that the radius of the plastic volume around an indenter is roughly ten times the radius of the indentation; Lawn's theory relates the radius with the diagonal length of the indentation, the semi-angle of the indenter and the material's elastic modulus and hardness by:

$$\frac{b}{a} = \left(\frac{E}{H}\right)^{1/2} ctg^{1/3}\varphi \tag{1}$$

Table 1
Details of specimens used for evaluations.

Evaluations	Materials	Amounts	Dimensions			Deposition pattern
			Length (mm)	Width (mm)	Thickness (mm)	
Elastic modulus	Metco 308NS	3	50	12	Each material was produced with three thicknesses, 2.1, 2.4, 3, exclusive of substrate 0.16, 0.11 1.62	On both sides
	Metco 313NS	3	50	12		
	Metco 601NS	3	50	12		
	308 + Bondcoat	3	50	12		
	313 + Bondcoat	3	50	12		
	601 + Bondcoat	3	50	12		
	Bondcoat	2	50	12		
	Substrate	1	50	12		
Hardness	Metco 308NS	3	10	12	Each material was produced with three thicknesses, 2.1, 2.4, 3, exclusive of substrate	On one side
	Metco 313NS	3	10	12		
	Metco 601NS	3	10	12		
Ultimate tensile strength	Metco 308NS	1	50	12	3 for all exclusive of substrate	
	Metco 313NS	1	50	12		
	Metco 601NS	1	50	12		
Scratch test	Metco308NS	1	15	12	2.1 for all exclusive of substrate	
	Metco313NS	1	15	12		
	Metco601NS	1	15	12		

In which b is the radius of the plastic volume, a is the half diagonal length of the indentation. E and H are the elastic modulus and hardness of the tested film. φ is the indenter semi-angle. Although the hardness of abradable seal coating materials is primarily evaluated by the R15Y test [4,20], in our work microhardness evaluation was conducted using a Mitutoyo model HM-101 microhardness tester, which has been detailed in the investigation paper [4]. To calculate the plastic region both approaches were followed and results were compared.

2.3. Ultimate tensile strength evaluation

Abradable coating materials are mechanically weak in tension and it is not possible to debond them as intact coatings from the substrates for UTS evaluation. A method was therefore found to assess the coating UTS with the coatings remaining on the substrates.

When the load is applied to the specimen, it is supported by both the coating and the substrate. However, when the coating is relatively weak, as is the case here, the influence of the substrate in supporting the load is obviously greater. Failure of a coating-substrate composite system can occur due to either tensile cracking or delamination, depending on adhesion [21].

One of the two failure modes occurs eventually in the tensile test; whichever occurs first depends on the relative strengths and the adhesion between the coating and substrate [21]. Abradable coatings have porous structures and low UTS values [5], and are thus more likely to fracture prior to major coating delamination. The coating fractures abruptly whereas the detachment of coating takes place progressively. Therefore the load-extension curve was expected to represent a sudden drop as the coating breaks, followed by a period of instability corresponding to gradual coating detachment.

The experiment setup and calculation procedures are detailed in the investigation paper [4]. All the samples were pulled until failure and load-extension curves were recorded by the tester at each 0.02 mm of extension.

2.4. Progressive Abradability Hardness (PAH)

The PAH may also be termed 'specific energy' [12] or alternatively, 'specific grooving energy' [10] (since it is defined as the work done per volume of abraded material), and can be measured by scratching a stylus across a surface. Its value is given by

$$H_a = \frac{W}{V} \tag{2}$$

where H_a is the PAH, W is the energy consumed during the scratching process (i.e., the work done by the scratching stylus) and V is the groove volume. The term measures how difficult it is to abrade a material in terms of the energy needed to produce scratch grooves. Materials that have high abradability have low PAH values and vice versa [9,10,12]. This concept was put forward in a slightly different form by Vingsbo and Hogmark [22], who described the specific energy as a quantitative indication of the abrasion resistance of steels. Vingsbo suggested the specific energy be more accurately obtained by dividing the energy by the mass loss. Later, in the 1980's the energy-dissipation concept was used for measuring the abradability of gas path sealing by Kennedy and Hine [10] and a single-pass pendulum apparatus was implemented as it provided a relatively fast, impact-like rubbing process where the energy consumed in the process could readily be assessed from the swing angles before and after the scratching. They evaluated the groove volume rather than mass loss as the latter was difficult to measure and groove volume was related more directly to the deformation created.

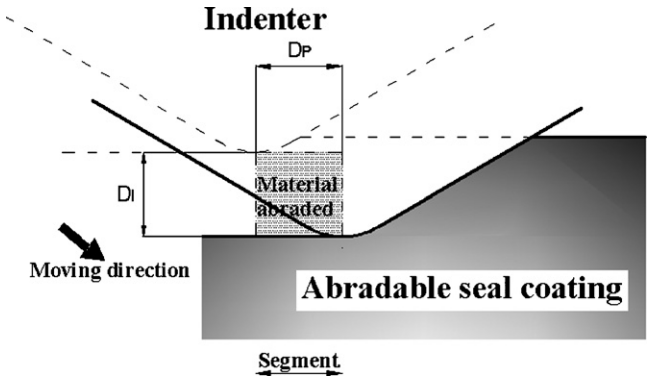

Fig. 2. The moving indenter and its displacements.

During our scratch tests, forces in both normal and transverse directions, displacement of the indenter and acoustic emission were recorded by the controlling unit at a sampling interval of 0.1 mm, enabling the calculation of energy consumed and groove volume produced by the stylus. Fig. 2 shows the rationale of the method.

The PAH can be expressed as

$$H_a = \frac{\sum_{i=1} F_{Ti} \cdot D_{Pi} + \sum_{i=1} F_{Ni} \cdot (D_{i+1} - D_i)}{\sum_{i=1} A_i(D) \cdot D_{Pi}} \quad (3)$$

where F_T and F_N are the tangential force and normal force recorded by the scratch tester. D_P and D_i are the ploughing and indentation displacement of the indenter. D is the indentation depth and A is the groove cross section area that is a function of the indentation depth, and is used to calculate the groove volume. The subscript "i" indicates parameters for the ith discretised segment.

A detailed description of this model has been given in the investigation paper [4]. In an attempt to determine the coating material abradability, a CSM Instruments Revetest Scratch Tester was used to scratch the samples in a controlled, relatively slow manner that applied a progressively increasing normal load to the samples. A Rockwell C 120° diamond cone with a 200 μm tip radius was used as the slider that was drawn across the samples at a constant speed of 10 mm/min. An acoustic sensor attached to the load arm was used to detect the acoustic emission during scratching. An initial screening trial stage was performed in the first place to define a maximum usable load so that no gross coating spallation would occur. Considering the geometry and a moderate loading rate, two end loads (50 N and 100 N) were evaluated in the screening trial stage to make sure the adhesion critical load would not be reached during the actual scratch testing.

No observable sudden changes of frictional force were detected by the transducer at either load, and this showed all the samples were not prone to adhesive failure during the tests. Therefore, the following loading procedure was carried out on all the samples, producing five scratch grooves with lengths of 0.9 mm, 2.9 mm, 4.9 mm, 6.9 mm and 9.9 mm on each sample. The five grooves were kept 1.5 mm apart and parallel to each other. A 1 N initial load was applied to enable the starting point to be clearly distinguished. The loading was increased progressively at a rate of 100 N/min, making the end loads 10 N, 30 N, 50 N, 70 N and 100 N. All six scratched samples were then examined by SEM.

2.5. Coatings

The three abradable coating materials were plasma sprayed using standard equipment to Sulzer Metco proprietary spraying parameters. Their compositions (from datasheets [20,23,24]) are specified in the investigation paper [4].

Metco 308NS is based on nickel–graphite cermet powder with a microstructure of a continuous nickel matrix embedded with a graphite solid lubricant and a controlled amount of pores [20]. Metco 313NS uses an aluminium silicon alloy–graphite composite powder with microstructure of a continuous aluminium silicon alloy matrix with graphite and porosity uniformly distributed throughout [23]. Metco 601NS is a blend of aluminium, silicon and polyester powder. The microstructure is a continuous aluminium silicon alloy matrix with dispersion of polyester particles, which provide abradability and a low friction coefficient [24]. The Metco 450NS bondcoat consists of a nickel–aluminium alloy matrix (80Ni–20Al wt.%) and was deposited by thermal spraying beneath the abradable coatings to enhance bonding. Coating materials were sprayed on low alloy steel strips of different sizes. The elastic modulus (E) of the steel strips was 172.4 GPa, and the Vickers hardness was 171 H_v (kgf/mm^2).

3. Results and discussion

3.1. Elastic modulus evaluation

The results for elastic modulus evaluations are shown in Table 2. The results show a decrease in the elastic modulus from Metco 308NS to Metco 313NS to Metco 601NS, all of which have extremely low elastic moduli compared to the substrate and the Metco 450 NS bondcoat. It is also shown that measured elastic moduli become lower at higher loads (Table 2). This could be attributed partly to plastic deformation of the samples, suggested by the fact that at higher loads the index of the dial gauge did not always rotate back to the starting point. Although pre-test calculation had been performed to ensure that no major plastic deformation would take place, considering the multi-phase structure of abradable coatings, certain phases, i.e. graphite or polyester, might still have plastically deformed, leading to this low measured elastic modulus phenomenon at high loads. No dependency between elastic modulus values and abradable coating thickness was evident. A clear increase of measured elastic modulus was found when bondcoats were present.

3.2. Microhardness evaluation

Metco 308NS has the highest microhardness readings, followed by Metco 313NS and then Metco 601NS. All three candidate materials show different hardness readings with different applied loads as shown in Fig. 3. This is likely to be due to the fact that the proportion of phases contained in the sampled area (indentation) might vary and thus the contribution of a given phase to each reading can differ. This is supported by the fact that towards higher loads the scatter of microhardness readings decreases as the indenter samples more material. However, Metco 308NS was observed to show decreased hardness at the higher load, attributable to the indentation size effect [21] due to a greater proportion of elastic recovery of the indentation at lower loads. Note that before the finalisation of the hardness values each indentation had to be evaluated to determine whether there was likely to be a substrate influence on the reading, resulting in a 'composite hardness' effect. The results of the predicted plastic regions beneath the indenter are shown in Table 3.

Since the thinnest coating thickness was 2.1 mm, no indentation led to any "composite hardness effect", according to both the rule of thumb and Lawn's expression. Note the "one tenth" rule of thumb predicts much smaller plastically deformed volumes than the theory of Lawn.

A possible explanation of the difference between three approaches is that the theory by Lawn [19] is more suitable for

Table 2
Results of elastic modulus evaluation (bc = bondcoat).

Applied dead weight (N)	Substrate	Metco 450NS	Metco 308NS	Metco 313NS	Metco 601NS	Metco 308NS + bc	Metco 313NS + bc	Metco 601NS + bc
	Elastic modulus (GPa)							
1.88	158.3	269.5	4.4	3.8	2.5	4.9	4.7	3.5
3.76	180.9	260.4	4.5	3.2	2.2	4.1	3.7	2.7
9.8	178.0	239.6	2.8	2.3	1.6	4.2	3.3	1.9

materials with a low Y/E ratio, e.g. stainless steel and other non work-hardening materials and the rule of thumb is usually used for hard, brittle coatings (most likely ceramic coatings) that have high Y/E ratios. Abradable materials exhibit extremely low elastic moduli, making them materials with high Y/E ratios along with work-hardenable metals, ceramics and glasses, but their response to mechanical loading is obviously different to these materials due to soft and loose structure. A comparison of their relevant properties is given in Table 4 [25] (elastic moduli of abradable seal coatings are taken from measurements; compressive yield strength is taken as one third of the Vickers hardness from microhardness measurements).

The actual deformation mechanisms of abradable coatings can be illustrated by comparing how materials with high and low Y/E ratios behave under mechanical loading. Johnson [26] and Tabor [27] described different deformation responses to Vickers hardness measurement, shown Fig. 4. Tabor's theory pointed out that the material surface would pile-up at either side of the indenter, and the geometry of the pile-up was determined by the normal and friction stress between the indenter and the sampled material, which can be analysed by the slip line field within the plastic zone. This theory was suggested to be applicable for materials with low Y/E ratios. Johnson's expanding spherical cavity model described a different situation that is applicable to materials with high Y/E ratios. It was believed that only when a hydrostatic core existed beneath the indenter could plastic deformation take place prior to cracking, outside which was an elastic region that surrounded that hydrostatic core. However, we believe that neither of the two scenarios can well describe the behaviours of abradable seal coatings. No hydrostatic core is needed for accommodating plastic deformation, and the stress-concentrated edges of the indentation simply densify rather than pile-up; on the other hand, an elastic hinterland should exist due to high Y/E ratios. Therefore, the true plastically deformed regions of abradables were believed to lie in between that predicted using rule of thumb and the theory of Lawn.

3.3. Ultimate tensile strength evaluation

The load-extension curves were recorded by the tester every 0.02 mm, as shown in Fig. 5. Points A, E, G are where fracture was observed to occur for Metco 308NS, Metco 313NS and Metco 601NS, respectively, after which the coatings were gradually detached until fully debonded from the substrate at points B, F, H. Metco 313NS debonded earlier than Metco 308NS with a smaller extension at point F. The rest of curves behave similarly, indicating substrate extension, except for Metco 601NS that shows an abrupt drop of load, corresponding to an observed coating break within the grips.

It is worth noticing that in the vicinity of an extension of 1.5 mm, all the coatings failed. The extension at these coating fracture points largely exceeded the maximum elastic extension of the mild steel substrate, indicating the substrate must have plastically deformed by the time that these fractures occurred, therefore the load the substrate supported was considered as the product of its flow stress and the instantaneous cross-sectional area. The ultimate tensile strength evaluation shows a decreasing tendency from Metco 308NS to Metco 313NS and finally to Metco 601NS, as for the elastic modulus and the microhardness.

The ultimate tensile strength of each material was thus determined, as shown in Table 5.

3.4. Scratch testing

3.4.1. PAH measurement

Since the PAH is defined as the work done per unit volume of material abraded, any increase in PAH reflects a real increase in scratching resistance [4,12].

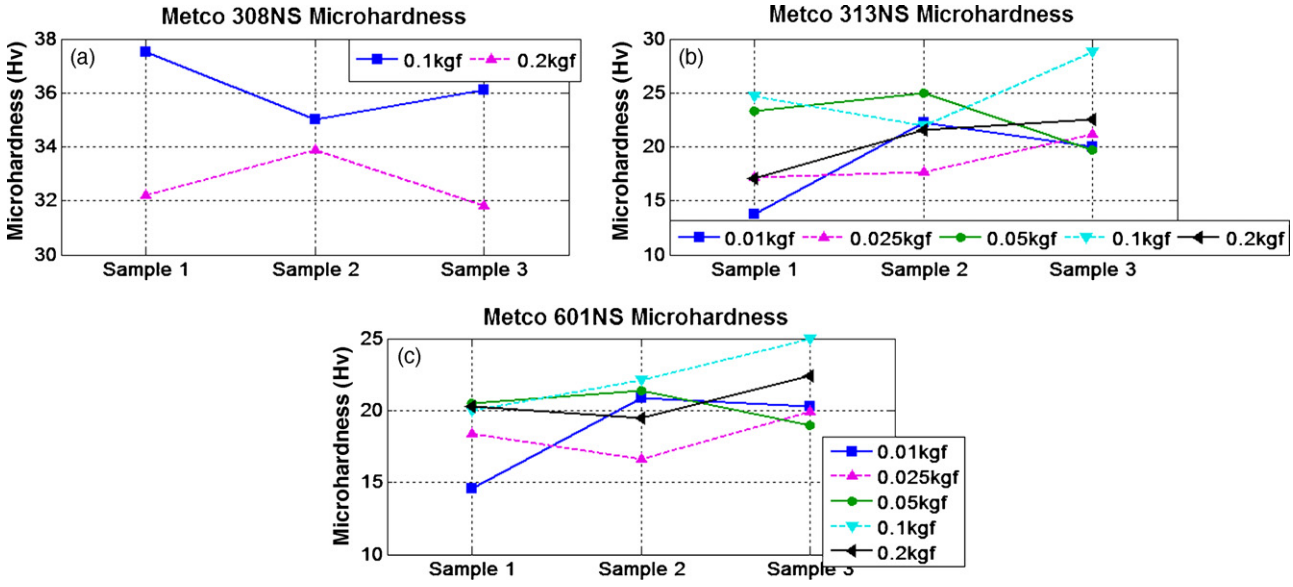

Fig. 3. Microhardness results in terms of the coating thickness (sample 1: 2.1 mm thickness of coating; sample 2: 2.4 mm thickness of coating; sample 3: 3 mm thickness of coating) and load. (a) Metco 308NS; (b) Metco 313NS; (c) Metco 601NS.

Table 3
Predicted plastically deformed region sizes.

Material	Load (kgf)	Plastic region radius (mm)	
		Rule of thumb	$\frac{b}{a} = \left(\frac{E}{H}\right)^{1/2} ctg^{1/3}\varphi$ (Lawn et al. [19])
Metco 308NS	0.1	0.113	0.316
	0.2	0.164	0.460
Metco 601NS	0.01	0.046	0.119
	0.025	0.075	0.194
	0.05	0.097	0.253
	0.1	0.132	0.344
	0.2	0.194	0.505
Metco 313NS	0.01	0.047	0.142
	0.025	0.071	0.217
	0.05	0.092	0.283
	0.1	0.127	0.388
	0.2	0.197	0.603

Table 4
Mechanical properties of various materials.

Material		Elastic modulus (GPa)	Compressive yield strength (MPa)	Yield strength (MPa) /Elastic modulus (GPa)
Ceramics	SiN	310	570	1.8
	SiC	430	820	1.9
Glass	96% silica glass	72	240	3.3
Abradable coating materials	Metco 308NS	3.95	11.3	2.9
	Metco 313NS	3.11	7.4	2.4
	Metco 601NS	2.08	6.9	3.3
Metals	Aluminium, bronze	120	33	0.3
	Heat treatable 4340 steel	207	120	0.6

It can be seen from Fig. 6 that Metco 308NS shows a clearly increasing PAH when the scratch length was increased. Metco 601 however, shows a rather stable PAH whereas Metco 313 is in between. The increase of the PAH at long scratches is attributed to coating densification and, possibly, a work hardening effect, which is a result of their different microstructures and compositions. The stable PAH of Metco 601 suggests that no densification From the microstructure point of view, Metco 308NS has the highest amount of porosity (15 vol%) that can accommodate material densification during scratching whereas Metco 601NS has the least (5 vol%); In terms of composition, a large amount of metallic phase (85 vol%) in Metco 308NS can be a source of work hardening.

Three abradable coating materials with bondcoats represent very similar PAHs which are considerably smaller than for samples coated only with abradable coatings. Furthermore, rather than being densified, their PAHs decrease towards higher loads and longer scratch lengths. Their acoustic emission curves were also found to be very smooth (not shown here), suggesting the primary accommodation mechanism was plastic deformation. This observation was unexpected and is believed to be due to a different stress field around the stylus induced by the bondcoats.

3.4.2. SEM scratch surface topography examination

Scratch surface topography is a good indicator of the underlying deformation mechanisms. All the scratch grooves were examined under SEM; it was noticed that scratch grooves on the same sample had almost identical appearances. There was no gross coating spallation detected, as it had been eliminated by the screening trial stage, and this is inconsistent with the stable frictional force. The acoustic emission, however, shows occasional peaks, indicating that both plastic deformation and coating fracture were present during the scratching.

As discussed before, Metco 308NS was densified considerably during scratching, leading to a great increase in PAH. Its scratch topography is smooth and dense, and there is no evidence of coating fractures, as shown in Fig. 7.

The darker graphite colonies were dislodged and dragged along the scratch, and the removed graphite debris was crushed beneath the stylus into the nickel matrix, again leading to densification. The relatively high strength of Metco 308NS leads to a greater constraining effect of the undeformed material to the pressurised material beneath the stylus, which adds to densification. However, cracking was observed along the nickel–graphite interfaces and within the graphite colonies where the bonds are relatively weak, and those cracks account for minor peaks and valleys in the acoustic emission curve. They appear in the grooves as concentric semicircle, which is typical of tensile cracks. As the slider scratches the surface, the normal and tangential stresses produce excessive tensile stress at the rear part of the contact spot, as well as the edges of the groove, therefore material behind the contact is fractured due to very low ultimate tensile strength [28]. Conformal cracks that usually occur because of buckling of material in front of the slider were not observed on any of the samples, due to the fact that the loose structure can accommodate large compressive stress prior to failure.

In comparison, more tensile cracks were observed on Metco 313NS surface, as shown in Fig. 8. The appearance of Metco 313NS groove shows a topography that is apparently less dense, in agreement with the PAH. Unlike the Metco 308NS, the cracks are

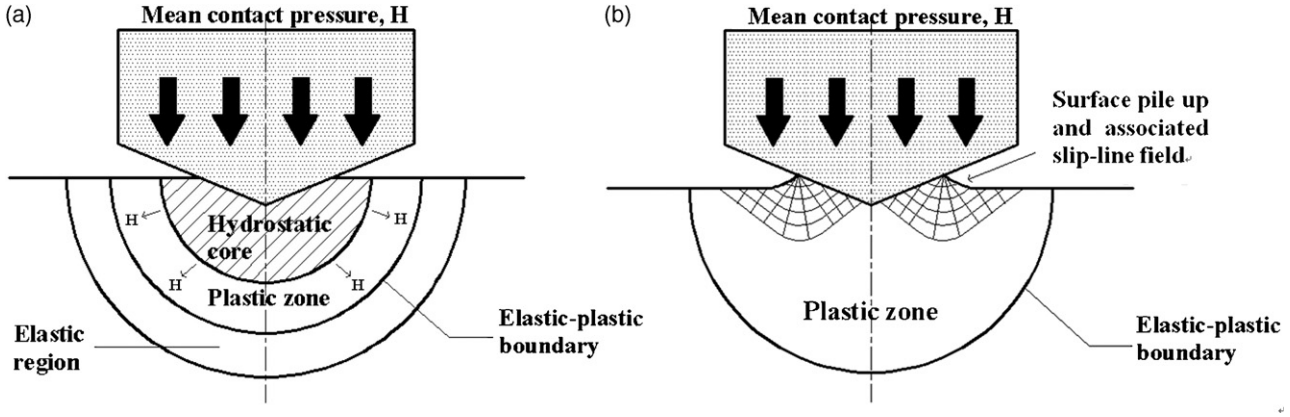

Fig. 4. The two deformation modes encountered during indentation: (a) Johnson's modification of the expanding spherical cavity model for materials of higher Y/E; (b) Tabor's surface pile-up model.

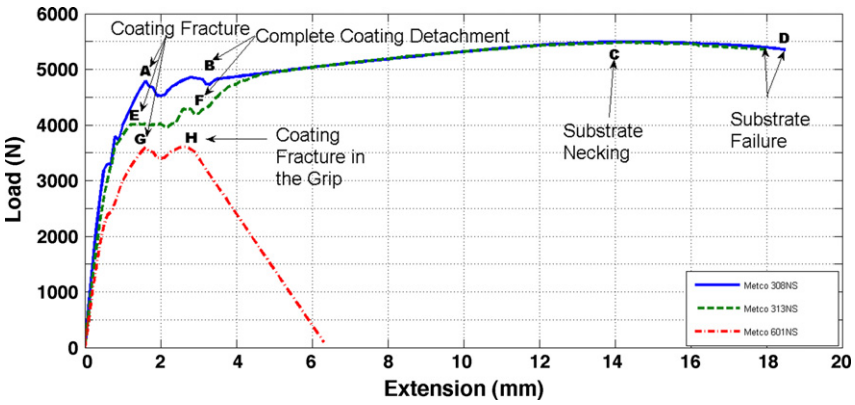

Fig. 5. Load-extension curves during the UTS evaluation.

Table 5
Ultimate tensile strength evaluation results.

Materials	Coating cross-section area (mm^2)	Maximum loading registered (N)	Maximum coating load (N)	UTS (MPa)
Metco 308NS	16.5	4883	1459.2	48.6
Metco 313NS	16.5	4118	694.3	23.1
Metco 601NS	16.5	3682	258.3	8.6

not confined along the aluminium-graphite interfaces but extend within the aluminium matrix. This is attributable to the low strength of the aluminium matrix coupled with a large amount of graphite (up to 22 vol%).

Metco 601NS has a completely different groove topography from the other two, as shown in Fig. 9. In situ coating spallation and chipping were observed both within the groove tracks and along the edges on Metco 601NS. This indicates that when the samples were scratched, the material ahead of the stylus was fractured and spalled due to a low compressive strength, as determined by the experiments. However, the rather large coating thickness ensured that coating detachment from the substrate did not occur. This morphology can be further attributable to the different responses of the aluminium matrix and polyester solid lubricant phase. Polyester has extremely low flexural strength and elastic modulus; as a result the stored energy tends to induce considerable elastic recovery (as opposed to the aluminium matrix). Chipping was found both within the track and at the groove edges, suggesting that chips were removed and crushed back into the track. The rather flat chipping morphology signifies that the collapsed material was pressed by the passing stylus, as shown in Fig. 9. Since most of the material collapsed and spalled ahead of the stylus instead of undergoing plastic deformation, there is no indication of densification, resulting in a rather stable PAH. The amount of acoustic emission can be directly related to cracking during deformation, which is shown in Fig. 10 [4]. It can be found that the acoustic emission of Metco 601NS was remarkable and unstable during the scratching, indicating the onset of crackings. Metco 308NS on the other hand showed a very stable and much smaller acoustic emission.

Another possible explanation of the low PAH detected for Metco 601NS could be related to a finding by Maozhong Yi et al. [8], who stated that a complete film layer, containing carbon and oxygen diffused from the polyester, was found adhered to the counterpart ring in a block-ring wear testing. This film decreased the friction coefficient. Since such a friction reduction would decrease the energy consumed in the scratching process, this would also decrease the PAH. In our tests the polyester was smeared onto the tool, leaving a surface topography as shown in Fig. 9.

It is worth noticing that when a Metco 450NS bondcoat was added in between the coatings and the substrates, all the three samples have a rather smooth and dense scratched topography, with less cracking present. The stable and limited acoustic emission proves this, and the reason, as stated before, is due to the compressive stress that the bondcoat imposed on to the abradable materials which retarded crack propagation, especially in regions that were subject to tensile stress and would have otherwise fractured.

3.4.3. SEM scratch cross-sectional topography

The specimens were also sectioned and examined under an SEM, as shown in Fig. 11.

Dominant deformation mechanisms were distinguished, e.g., whether the deformation was accommodated by coating fracture or plastic deformation. As a result of the scratching slider, plastic deformation led to densification, characterised by crushed layers of materials, e.g., deformed pores and graphite colonies. The materials were squeezed and aligned in a parallel pattern.

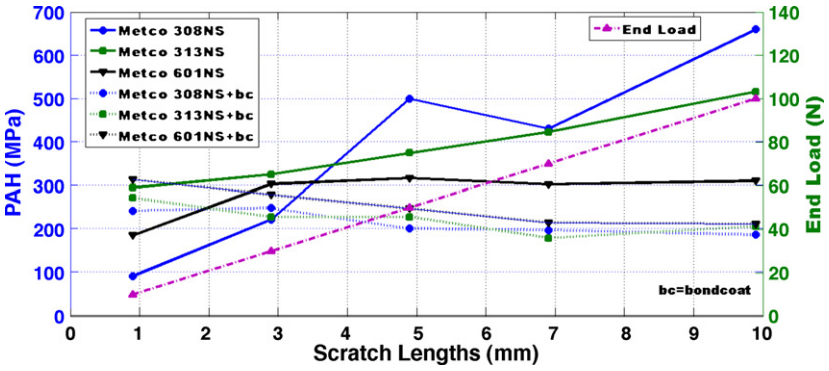

Fig. 6. PAH measurements.

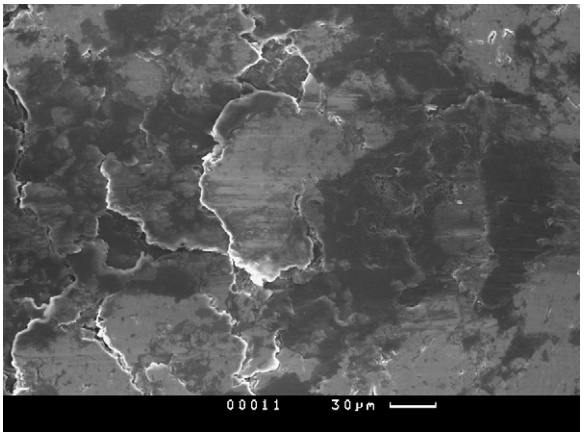

Fig. 7. Metco 308NS Scratch groove topography.

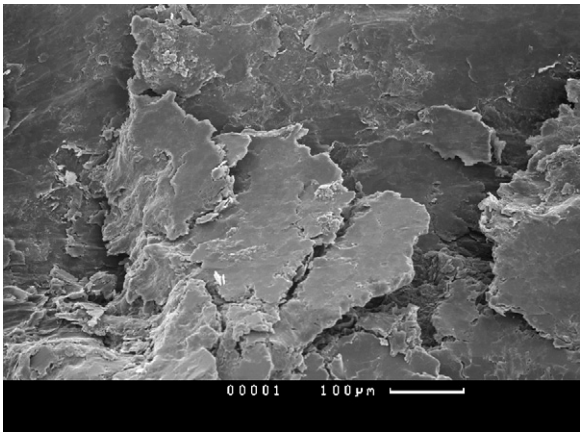

Fig. 9. Metco 601NS Scratch groove topography.

Fig. 11(a) and (b) illustrate that in the case of Metco 308NS, a considerable amount of material beneath the drawing stylus underwent plastic deformation resulting in significant densification. Metco 308NS without a bondcoat beneath showed obvious evidence of densification, but the densified region was constrained in a smaller volume, compared to that with a bondcoat. Hardly any porosity can be found in the adjoining densified regions but they gradually become visible further beneath. Conversely, porosity can be seen through the whole picture where there is a bondcoat added underneath. The pores, however, are squeezed and deformed into the shape coinciding with the stylus profile, but are still visible, indicating a reduced degree of densification but a larger region affected.

The expected densification regions are almost invisible in the pictures of Metco 313NS since most of the pores beneath the stylus remain round-shaped and are evenly distributed, even in areas close to the groove edges, as shown in Fig. 11(c) and (d). This is however contradictory to the scratch surface topography and the PAH, both indicating there should have been some regions where densification took place.

Fig. 11(e) shows no indication of plastic deformation and densification of Metco 601NS, but instead there are cracks present both within the aluminium matrix and the aluminium-polyester interfaces. In the pictures of coatings with bondcoats, as shown in the right column, cracks are largely reduced and become virtually unobservable. The polyester becomes aligned conforming to the stylus profile. This shows that Metco 601NS with a bondcoat indeed underwent some level of plastic deformation and the level of coating fracture was reduced by the bondcoat. The reason for the bondcoat effectively decreasing the PAH and densification is not fully understood, but we speculate that the bondcoat enhances the interfacial stiffness and will have altered the stress field beneath the stylus.

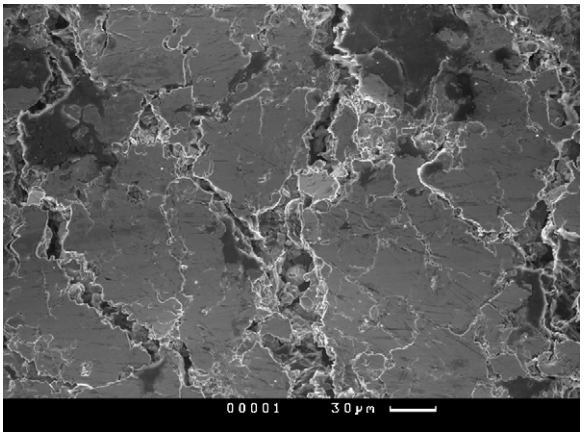

Fig. 8. Metco 313NS Scratch groove topography.

3.5. Measure of abradability

Previous papers using erosion systems [6] and sliding wear test [8] suggested a material's abradability could be related to other mechanical properties such as hardness and ultimate tensile strength. Instead, the PAH has been proposed in this paper as an indicator of scratch resistance. The PAH can reflect the material's abradability such that: (1) a high PAH indicates low abradability and vice versa; (2) an increasing PAH indicates densification, and is thus also an indication of abradability. PAH has also been shown to be influenced by other mechanical properties. Metco 308NS has the highest elastic modulus, microhardness and ultimate tensile strength, followed by Metco 313NS and Metco 601NS. This influence is related to the degree of densification. It can be clearly found that when the hardness, elastic modulus and ultimate tensile strength increase, the PAH shows a large increase when tested at longer scratches, suggesting a decreasing abradability, as shown in Fig. 12. Metco 308NS has a large variation of PAH at different scratch lengths, showing a considerable amount of densification, followed by Metco 313NS and Metco 601NS. As stated and interpreted before, it is believed that the degree of densification has a link with these other mechanical properties. A material's intrinsic properties and its response to scratching, e.g., fracture or densification, in conjunction, determine its abradability and abrasion or erosion resistance.

It is also suggested that when rating abradable seal coatings, both points (1) and (2) mentioned above have to be considered. Point (2) is more relevant with material's dynamic behaviour and is worth studying. Therefore, an important point is that in order to study how the coatings react dynamically under scratching, their progressive behaviours have to be measured by either: (1) performing multiple scratching processes with different lengths and measuring the average PAH of each scratch lengths; (2) performing single scratching but progressively measuring the PAH.

3.6. Results compared to test-bed findings

The conditions in which our experiments were performed were very different from actual engine operation, i.e., our results of the abradability were obtained at much lower strain rates. However, by comparing our results with technical datasheets provided by

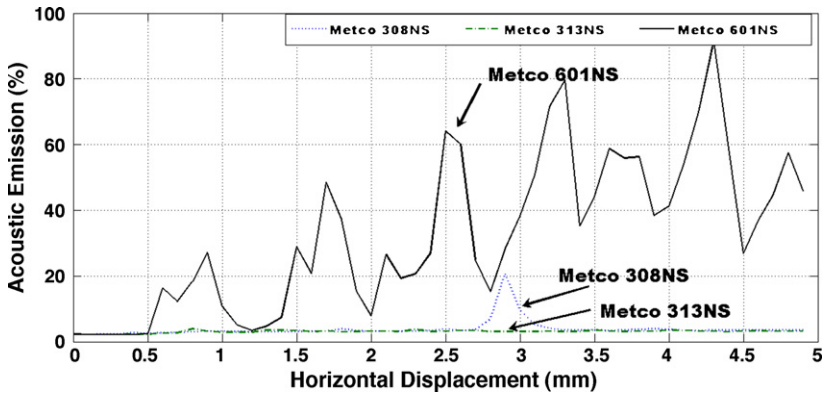

Fig. 10. Acoustic emission of abradable coating materials during 4.9 mm scratching.

Sulzer Metco Ltd., it is found that similar conclusions have been drawn [20,23,24]. The datasheets provided by them suggest that the Metco 308NS coating has good erosion resistance but moderate abradability [20]. This is mainly due to the greater proportion of nickel matrix and the limited amount of graphite and porosity. The Metco 313NS is claimed to possess a balance of abradability and erosion resistance [23]. The Metco 601NS [24] is claimed to have a high degree of abradability with essentially no blade tip wear,

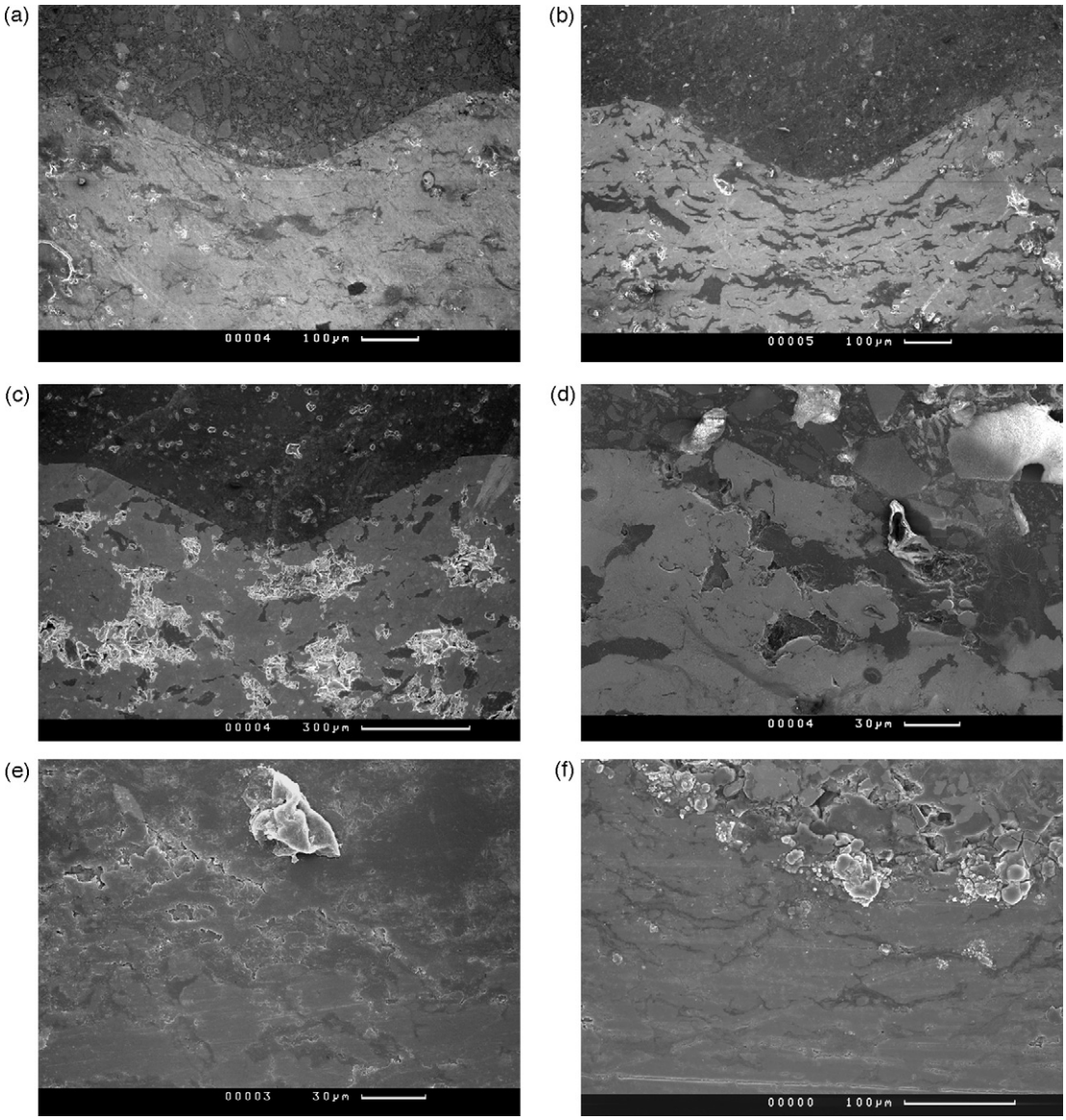

Fig. 11. Scratched groove cross-sectional appearance: (a) Metco 308NS; (b) Metco 308NS + bondcoat; (c) Metco 313NS; (d) Metco 313NS + bondcoat; (e) Metco 601NS; (f) Metco 601NS + bondcoat.

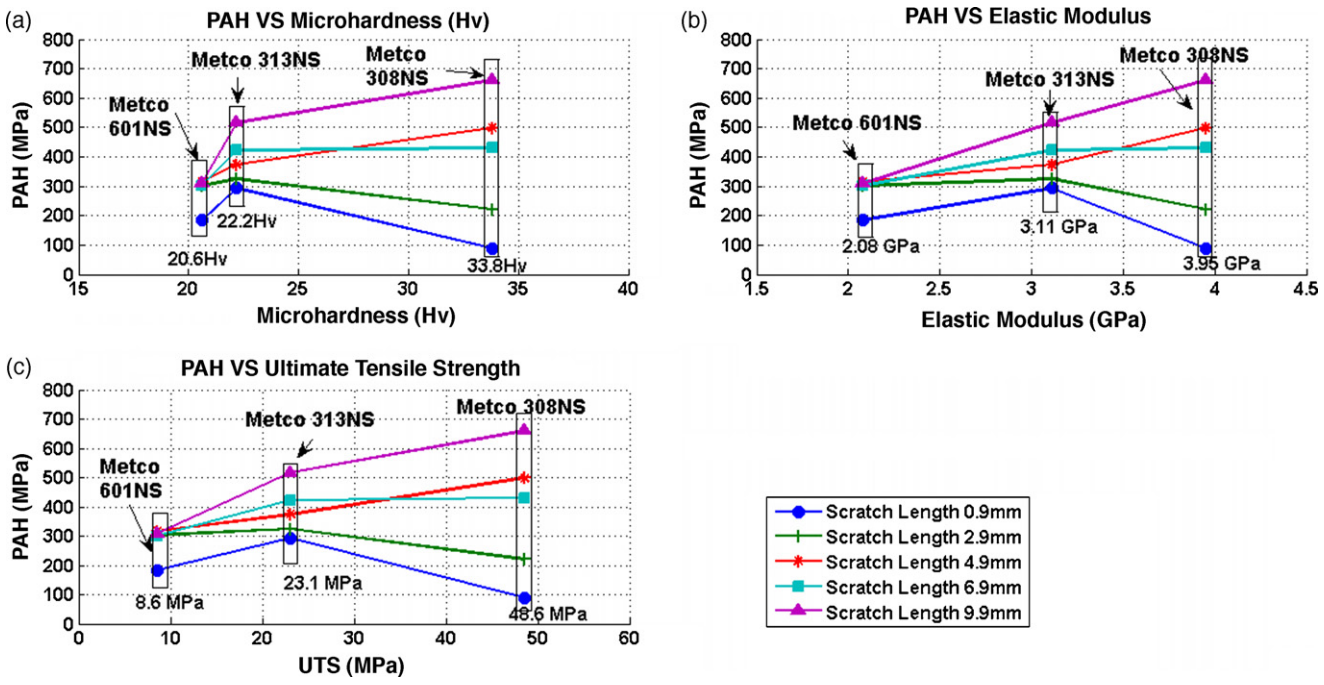

Fig. 12. Relation of PAH to other mechanical properties.

excellent oxidation resistance up to a temperature of 345 °C and good resistance to thermal shock. Therefore, although the scratch testing can by no means replicate the actual operating conditions of a gas-turbine engine, it gives reasonable results, thus it could be used as a cheap and easy laboratorial alternative to high speed test.

Wear resistance and abradability are opposing properties [6]. Therefore, conclusions can also be drawn regarding this property. The scratch tests indicate that Metco 308NS experienced considerable densification during the scratching that enhanced its wear resistance, which explains the fact that Metco 308NS is primarily developed for the compressor stages in turbine engines where extremely aggressive particulate matter is present and therefore erosion resistance is crucial [20]. In comparison, the Metco 601NS shows a rather low but stable PAH with virtually no densification taking place, which implies a good abradability but on the other hand poor erosion resistance. The Metco 313NS exhibits moderate PAH and densification halfway between that of Metco 308NS and Metco 601NS, and this could be an indicator of a desirable combination of both good abradability and erosion resistance.

The resemblance between the results of our evaluation on the abradable seal coatings and manufactures' qualitative conclusions suggests scratch testing could be an effective laboratory alternative to high speed engine rigs to determine a seal coating's abradability. The relationships between other mechanical properties and abradability indicate that the approach that was adopted is logical. However, it should be emphasised here that although these relationships between abradability and other mechanical properties such as hardness [6,8] and UTS [6] have been pointed out in previous papers, it was also suggested that none of these mechanical properties on their own can be used to rate and design abradable seal coating materials since abradability is also influenced by other factors such as composition and microstructure. Several exceptions to general mechanical properties relationships regarding hardness and abradability have been documented [6], suggesting measurements such as hardness and UTS can only be used as supportive experimental procedures. On the other hand, the success of abradable seal coatings depends on achieving an optimisation of two conversely related properties, the abradability and erosion resistance, and this is based on a full insight into the deformation mechanisms. Our approach using the scratch test is more revealing and is certainly superior to only using hardness or UTS as an indicator of abradability. Compared to other techniques involving specific grooving energy, i.e. the pendulum test, the scratch test enables the continuous study of material response to scratching, and the knowledge obtained can be used in optimisation of coating design.

4. Conclusions

(1) The PAH (Progressive Abradability Hardness) is demonstrated as an appropriate measure of coating abradability, as it is a direct indicator of the ease or difficulty with which the material can be abraded, though in a low speed test. It is influenced by factors such as material's intrinsic properties such as composition and microstructure, as well as deformation conditions.
(2) Results from the evaluations using scratch testing are in agreement with test-bed conclusions of abradability, and this proves that scratch testing maybe an effective alternative, while being a relative low cost method.
(3) Mechanical properties such as elastic modulus, hardness and UTS have been shown to have a relationship with the PAH measurement, but they should not be used alone for abradability evaluation.
(4) Metco 601 has the best abradability, followed by Metco 313NS and Metco 308NS, according to our results, which agrees with industrial conclusions.

Acknowledgements

For assistance in the sample provision the authors would like to express appreciation to Mr. D. Anderson and his staff at Plasma Coatings Ltd. We also thank Dr. J.C. Avelar-Batista Wilson and Dr. J. Housden of Tecvac Ltd. for assisting the authors in carrying out the initial scratch tests. Later scratch tests were carried out with the help and assistance of research staff in Professor J. de Hosson's group at Groningen University in the Netherlands, and we also appreciate that help. Thanks also to staff of Rolls-Royce plc.

and Sulzer Metco Ltd. for providing useful datasheets concerning the coatings tested.

References

[1] Rolls-Royce plc., The Jet Engine, 4th ed., Rolls-Royce Press, Derby, 1986.
[2] F. Ghasripoor, R. Schmid, M. Dorfman, Abradable coatings increase gas turbine engine efficiency, Materials World 5 (1997) 328.
[3] P. Dowson, M.S. Walker, A.P. Watson, Development of abradable and rub-tolerant seal materials for application in centrifugal compressors and steam engines, Sealing Technology 12 (2004) 5.
[4] X. Ma, A. Matthews, Investigation of abradable seal coatings, Surface and Coating Technology 202 (2007) 1214.
[5] M.A. Clegg, M.H. Mehta, NiCrAlbentonite thermal spray powder for high temperature abradable seals, Surface and Coatings Technology 34 (1988) 69.
[6] H.I. Faraoun, T. Grosdidier, J.L. Seichepine, D. Goran, H. Aourag, C. Coddet, J. Zwick, N. Hopkins, Improvement of thermally sprayed abradable coating by microstructure control, Surface and Coatings Technology 201 (2006) 2303.
[7] R.E. Chupp, F. Ghasripoor, G.D. Moore, L.S. Kalv, J.R. Johnston, Applying abradable seals to industrial gas turbines, in: 38th AIAA/ASME/SAE/ ASEE Joint Propulsion Conference and Exhibit, Indianapolis, USA, July 7–10, 2002, p. 1.
[8] M.Z. Yi, J.W. He, B.Y. Huang, H.J. Zhou, Friction and wear behaviour and abradability of abradable seal coating, Wear 231 (1999) 47.
[9] U. Bryggman, S. Hogmark, O. Vingsbo, Force and energy measurements during controlled grooving—a basic study of abrasive wear, ASLE Transactions 24 (1981) 449.
[10] F.E. Kennedy, N.P. Hine, Single-pass rub testing of abradable seal materials, ASLE Lubrication Engineering 38 (1982) 557.
[11] F.E. Kennedy, Single pass rub phenomena—analysis and experiment, ASME Journal of Lubrication Technique 104 (1982) 582.
[12] Y.N. Liang, S.Z. Li, S. Li, Evaluation of abradability of porous seal materials using a single pendulum scratch test, Wear 177 (1994) 167.
[13] D.W. Hetzner, Microindentation hardness testing of materials using ASTM E384, Microscopy and Microanalysis 9 (2003) 708.
[14] T.J. Bell, E.G. Thwaite, Recent developments in hardness testing and their implications for standardisation, CIRP Annals—Manufacturing Technology 48 (1999) 449.
[15] H. Buckle, Science of Hardness Testing and its Research Applications, Metals Park Press, Ohio, ASM, 1973, p. 453.
[16] B. Jonsson, S. Hogmark, Hardness measurements of thin films, Thin Solid Films 114 (1984) 257.
[17] P.M. Sargent, PhD Thesis, University of Cambridge, UK, 1979.
[18] P.J. Burnett, D.S. Rickerby, Assessment of coating hardness, Surface Engineering 3 (1) (1987) 69.
[19] B.R. Lawn, A.G. Evans, D.B. Marshall, Journal of American Ceramic Society 63 (1980) 574.
[20] Sulzer Metco®, Technical Bulletin #10-115, 2000.
[21] S.J. Bull, D.S. Rickerby, Evaluation of coatings, in: D.S. Rickerby, A. Matthews (Eds.), Advanced Surface Coatings, Blackie, London, UK, 1991.
[22] O. Vingsbo, S. Hogmark, Single-pass pendulum grooving—a technique for abrasive testing, Wear 100 (1984) 489.
[23] Sulzer Metco®, Technical Bulletin #10-285, 2000.
[24] Sulzer Metco®, Technical Bulletin #10-141, 2000.
[25] E.R. Booser, Tribolgy Data Handbook, CRC Press, New York, USA, 1997.
[26] K.L. Johnson, The correlation of indentation experiments, Journal of the Mechanics and the Physics of Solids 18 (1970) 115.
[27] D. Tabor, The Hardness of Metals, Clarendon, Oxford, UK, 1951.
[28] S.J. Bull, Failure modes in scratch adhesion testing, Surface and Coating Technology 50 (1991) 25.